# Flow pattern in forced two-dimensional turbulence on a rotating sphere

Toru Nozawa 野沢　徹（京大・理・地物）

Shigeo Yoden 余田 成男（京大・理・地物）

Department of Geophysics, Kyoto University, Kyoto 606-01, JAPAN

## 1   Introduction

Large-scale motions in planetary atmospheres are largely turbulent in space and time. Although the large-scale turbulent motions are actually three-dimensional, one can consider them to be nearly two-dimensional (2D) on a horizontal surface owing to the stratification of atmospheres and the rotation of planets. For example, synoptic-scale disturbances in the atmosphere have such quasi-2D turbulent characteristics as shown by Boer & Shepherd (1983) with a global atmospheric data set;energy spectra and transfer functions in the spherical domain have some features of an enstrophy inertial subrange for a high-wavenumber region of $n > 10$, where $n$ is the total wavenumber of the spherical harmonics.

A geophysical application of the 2D turbulence theory ( Kraichnan 1967 ; Leith 1968 ; Batchelor 1969 ) was firstly done by Rhines (1975) with a numerical model on a $\beta$-plane to investigate the effect of the rotation of planets on the 2D turbulence. He showed that the upward energy cascade ceases roughly at a wavenumber $k_\beta = \sqrt{\beta/2U}$, where $U$ is the r.m.s. velocity and $\beta$ the meridional gradient of the Colioris parameter $f$;the conversion from turbulence into Rossby waves takes place around the wavenumber $k_\beta$. He also found that the flow field becomes anisotropic and a zonal band structure emerges owing to the $\beta$-effect. Maltrud & Vallis (1991) numerically studied the forced 2D turbulence on a $\beta$-plane with a high-resolution model ( $256^2$ or $512^2$ grids ) under recent advanced computing facilities. In their experiments with low-wavenumber forcing, coherent vortices, which were found by Basdevant et al. (1981) and McWilliams (1984) in the numerical experiment on planar 2D turbulence, become weak while anisotropy of the flow field increases as the strength of the $\beta$-effect increases, although energy spectrum in the enstrophy-cascading range remains relatively unchanged ( steeper than $k^{-3}$ ). An energy spectrum nearly proportional to $k^{-5/3}$ was also observed in the energy-cascading range in the experiments with high-wavenumber forcing.

Williams (1978) reproduced a band structure similar to that of Jovian atmosphere in a numerical experiment on the forced 2D turbulence on a rotating sphere. Nozawa and Yoden (1994) did a series of numerical experiments with the same framework as Williams aiming at a methodical sweep in parameter space. When the amplitude of the stochastic vorticity forcing is not very small and the latitudinal wavenumber of the forcing is relatively small, a clear band structure which consists of alternating easterly and westerly jets emerges in the flow field. However, the numerical model has a cyclic boundary condition in longitudes of 45°, and the forcing function is anisotropic. Thus the obtained band structure might be influenced by the assumed longitudinal periodicity and the anisotropic vorticity forcing.

In this paper, we perform a series of numerical experiments on the forced 2D turbulence in a full spherical domain with a homogeneous and isotropic forcing at high wavenumbers. The sensitivity to the rotation rate and that to the choice of the random numbers for the forcing are studied in detail. The flow field, particularly the formation of the band structure, is investigated as well as the energy spectrum and the transfer function. The numerical procedure is described in section 2, and results are given in section 3. Discussion is given in section 4, and conclusions are given in section 5.

# 2 Model and experimental procedure

Two-dimensional nondivergent flow on a rotating sphere is governed by a vorticity equation :

$$\frac{\partial \zeta}{\partial t} + \frac{1}{a^2} J(\psi, \zeta) + \frac{2\Omega}{a^2} \frac{\partial \psi}{\partial \lambda} = \nu \left( \nabla^2 + \frac{2}{a^2} \right) \zeta + F , \tag{1}$$

where $\psi(\lambda, \mu, t)$ is a streamfunction field, $\zeta(\lambda, \mu, t) = \nabla^2 \psi$:vorticity, $\lambda$:longitude, $\mu$:sine latitude, $t$:time, $\nabla^2$:horizontal Laplacian, $J(\psi, \zeta)$:horizontal Jacobian, $a$:radius of the sphere, $\Omega$:rotation rate of the sphere, $\nu$:kinematic viscosity coefficient, and $F(\lambda, \mu, t)$:vorticity forcing function. The radius of the sphere is set to that of Jupiter;$a = 7.00 \times 10^7$m and the time $t$ is measured by Jovian day ; 1 J.day $= 2\pi/\Omega_J = 3.57 \times 10^4$s, where $\Omega_J = 1.76 \times 10^{-4}$rad s$^{-1}$ is the rotation rate of Jupiter. The kinematic viscosity coefficient of $\nu = 5.00 \times 10^5$m$^2$s$^{-1}$ is adopted in this study.

For the forcing function $F$, a random Markovian formulation is used as in Lilly (1969) and Williams (1978) :

$$F(\lambda, \mu, j\Delta t) = RF(\lambda, \mu, (j - 1)\Delta t) + (1 - R^2)^{1/2}\widehat{F}(\lambda, \mu, j\Delta t) , \tag{2}$$

where $R$ is a dimensionless memory coefficient ( $R = 0.98$ as in Williams (1978) ), and $\widehat{F}$ is a random vorticity source at every time step. Here the random vorticity source function is defined as follows :

$$\widehat{F}(\lambda, \mu, j\Delta t) = \sum_{n=n_{min}}^{n_{max}} \sum_{m=1}^{n} \widehat{F}_n^m(j) P_n^m(\mu) e^{im\lambda} , \tag{3}$$

where $\widehat{F}_n^m(j)$ is an expansion coefficient of $\widehat{F}$ with spherical harmonics, which is determined so that it has random amplitude and phase at every time step $j$ in order to construct a homogeneous and isotropic forcing under the restriction of $|| \widehat{F}(\lambda, \mu, j\Delta t) ||= \sqrt{\sum_{n=n_{min}}^{n_{max}} \sum_{m=1}^{n} | \widehat{F}_n^m(j) |^2} = F$ (constant). The forcing is given in a narrow range of $n_{min} = 77$ and $n_{max} = 81$ and the amplitude is held constant to F $= 7.85 \times 10^{-11}$s$^{-2}$ for all the experiments in this study. Figure 1 shows an example of the forcing field at a paticular J.day.

A pseudospectral method with a triangular truncation of T199 ( $n \leq 199 = N$ ) is used for the computation of the advection (Jacobian) term;grids for the spectral transformation are 600 in longitudes and 300 in latitudes. Equation (1) is integrated from an initial condition of zero velocity field for a period of 1000 J.days. The fourth-order Runge-Kutta-Gill method is used for the time integrations with $\Delta t = 0.05$ J.days. All of the computations are done in double precision.

As an experimental parameter, six values of the rotation rate are taken:$\Omega/\Omega_J = 0.00, 0.25, 0.50, 1.00, 2.00$, and $4.00$. The sphere has $\Omega/\Omega_J$ rotations par unit J.day. For each rotation rate, three runs are done with different random sequences for the amplitude and phase of the vorticity source function.
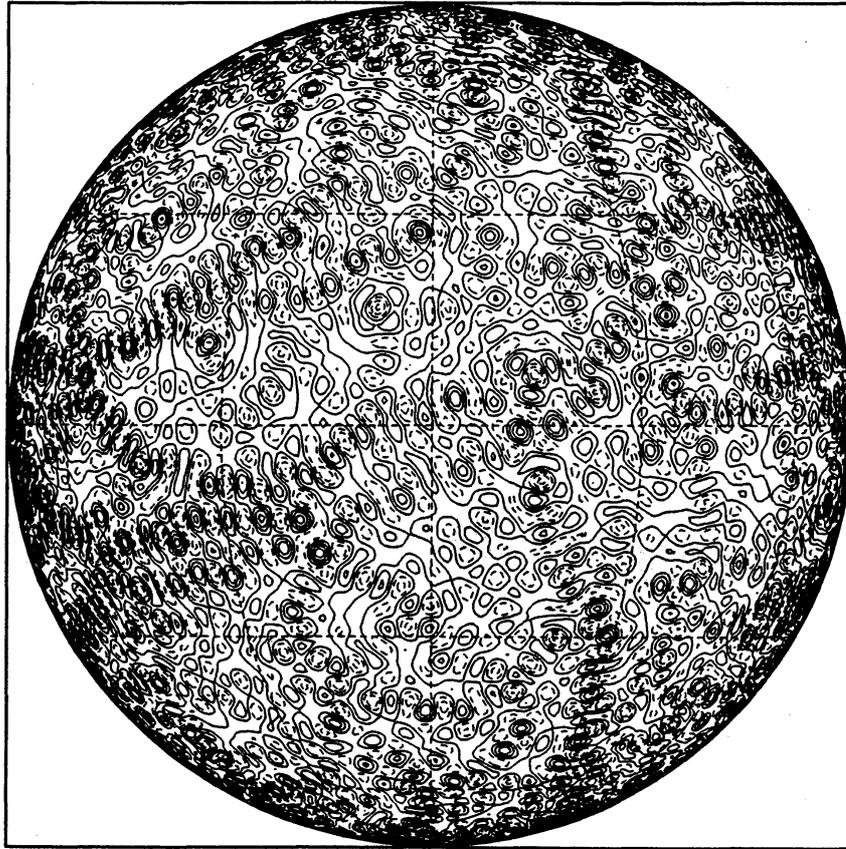
**Fig.1:** Vorticity forcing field at $t = 100$ J.days. Contour interval is $1.0 \times 10^{-10}$ s$^{-2}$ and negative areas are drawn by dotted lines.

# 3 Results

Figure 2 shows the time variation of the total kinetic energy $\mathcal{E}(t) = \sum_{n=2}^{N} E(n, t)$ and the total

enstrophy $\mathcal{Q}(t) = \sum_{n=2}^{N} Q(n, t)$ for six values of the rotation rate, which are ensemble averages of

three runs. Here the energy spectrum density $E(n, t)$ and the enstrophy spectrum density $Q(n, t)$ are, respectively, defined as follows :

$$E(n,t) = \frac{n(n+1)}{2} \sum_{m=-n}^{n} | \psi_n^m(t) |^2 , \tag{4}$$

$$Q(n,t) = \frac{n^2(n+1)^2}{2} \sum_{m=-n}^{n} | \psi_n^m(t) |^2 , \tag{5}$$

where $\psi_n^m(t)$ is an expansion coefficient of $\psi$ with spherical harmonics :

$$\psi(\lambda, \mu, t) = \sum_{n=2}^{N} \sum_{m=-n}^{n} \psi_n^m(t) P_n^m(\mu) e^{im\lambda} . \tag{6}$$

At the beginning of $t < 20$ J.day, both of the total energy and the total enstrophy increase sharply, growth rates of which are almost independent of the rotation rate. As the time goes by, the energy increases gradually while the enstrophy decreases. The energy is smaller for larger $\Omega/\Omega_J$, although it is not very different for the experiments with $\Omega/\Omega_J \leq 1.00$. On the other hand, the enstrophy is larger for larger $\Omega/\Omega_J$. Even at the end of time integrations ( $t = 1000$ J.day ), the total energy goes on increasing slightly while the enstrophy becomes nearly constant.
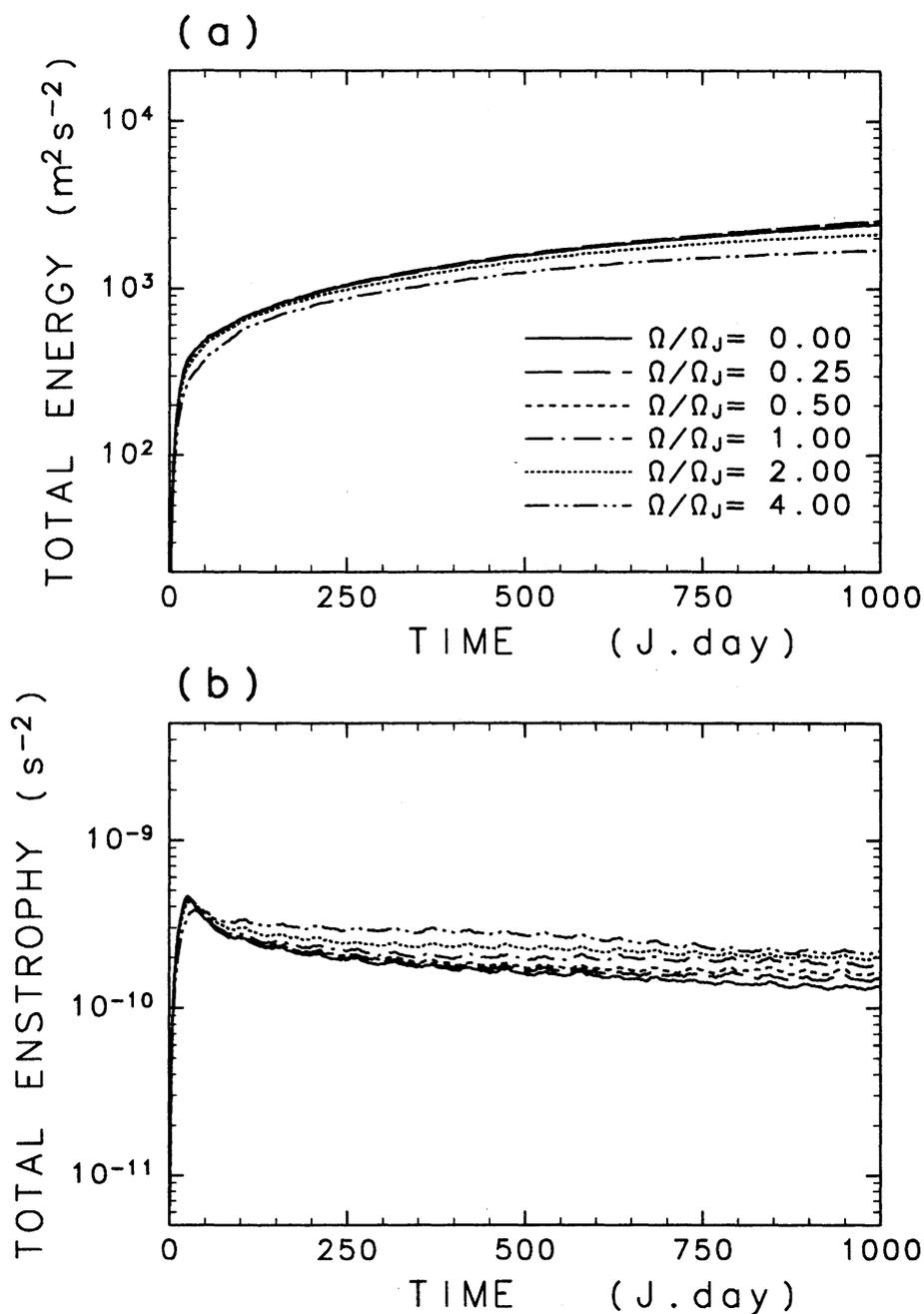


Fig.2: Temporal variation of the total kinetic energy $\mathcal{E}(t)$ (a), and the total enstrophy $\mathcal{Q}(t)$ (b) for six values of $\Omega/\Omega_J$. Ensemble averages of three runs.

Figure 3 shows the energy spectra for six values of $\Omega/\Omega_J$. These are time averages from 800 to 1000 J.days. Three runs are plotted for each rotation rate. A wavenumber $n_f$ indicates the forcing wavenumber: $n_f = \dfrac{n_{min} + n_{max}}{2} = 79$, which corresponds to the wavenumber of energy and enstrophy inputs. The power law of the energy spectrum is close to $n^{-4}$ in the enstrophy-cascading range, which slope is independent of the choice of the random numbers for each $\Omega/\Omega_J$. The slope in this range becomes a little gentle as the rotation rate increases, although it is yet steeper than $n^{-3}$ even for the runs with $\Omega/\Omega_J = 4.00$ (f).

For all the experiments, an upward energy-cascading range is obtained. The energy spectra are nearly proportional to $n^{-5/3}$ in the energy-cascading range, and the slope steepens slightly as $\Omega/\Omega_J$ increases. Three energy spectra of different random numbers are very similar in this range as well as those in the enstrophy-cascading range. In the case of no rotation (a),the energy spectrum is steeper than $n^{-5/3}$ At the low wavenumbers of $n \underset{\sim}{<} 5$ owing to the finiteness of the spherical domain. For the experiments with rotation (b-f), on the other hand, the spectrum does not obey the power law at low wavenumbers;the energy-cascading range becomes narrow and the energy spectrum in this range becomes noisy as $\Omega/\Omega_J$ increases. Here another wavenumber $n_\beta$ is introduced following to Nozawa and Yoden (1994) :

$$n_\beta \equiv a \sqrt{\frac{\langle \beta \rangle}{2U}} \, , \tag{7}$$

where $U$ is the r.m.s. velocity ( $U = \sqrt{2\mathcal{E}}$ ) at $t = 1000$ J.day (ensemble averages of three runs here), and $\langle \beta \rangle$ is the spherical average of $\beta$:$\langle \beta \rangle = \frac{1}{2} \int_{-1}^{1} \beta d\mu = \pi\Omega/2a$. At the horizontal scale of $a/n_\beta$, the nonlinear Jacobian term is comparable to the "$\beta$-term" in Eq.(1). Figure 3 shows that $n_\beta$ roughly gives the lower bound of the energy-cascading range. The spectrum does not show any clear power law in $2 \leq n \underset{\sim}{<} n_\beta$ (b-f), where the "$\beta$-term" is larger than the nonlinear term. In this range, the energy spectrum is very noisy and it depends on the choice of the random numbers. For larger $\Omega/\Omega_J$ (e,f), the energy density is relatively small at the lower wavenumbers in this range. This is why the total energy is relatively small for larger $\Omega/\Omega_J$ as seen in Fig.2 (a).

The energy flux function $\Pi(n, t)$ is calculated from the energy transfer function $T(n, t)$ :

$$\Pi(n, t) = \sum_{n'=2}^{n} T(n', t) \, , \tag{8}$$

$$T(n, t) = -\sum_{m=-n}^{n} \{\psi_n^m(t)\}^* N_n^m(t) \, , \tag{9}$$

where $N_n^m(t)$ is the expansion coefficient of the nonlinear Jacobian term, and $*$ denotes complex conjugate. Figure 4 shows the energy flux functions for six values of $\Omega/\Omega_J$, which are time averages from 800 to 1000 J.day and ensemble averages of the three runs. For the case of no rotation, the energy flux is nearly constant in the range of $2 \leq n \underset{\sim}{<} 20$, thus the energy is transferred as far as the lowest wavenumber of $n = 2$. When the rotation rate is small or moderate ($0.00 < \Omega/\Omega_J \leq 1.00$), the energy flux function in the range of $n_\beta \underset{\sim}{<} n \leq n_f$ is parallel to that of no ratation, indicating that the effect of the rotation is weak in this range. The energy flux in this range becomes large as $\Omega/\Omega_J$ increases because the energy density is larger for larger $\Omega/\Omega_J$ in this range as seen in Fig.3 (a-d). In the range of $2 \leq n \underset{\sim}{<} n_\beta$ the energy flux function is not parallel to that of no rotation, but it has a large decline;only a little energy is transferred to this
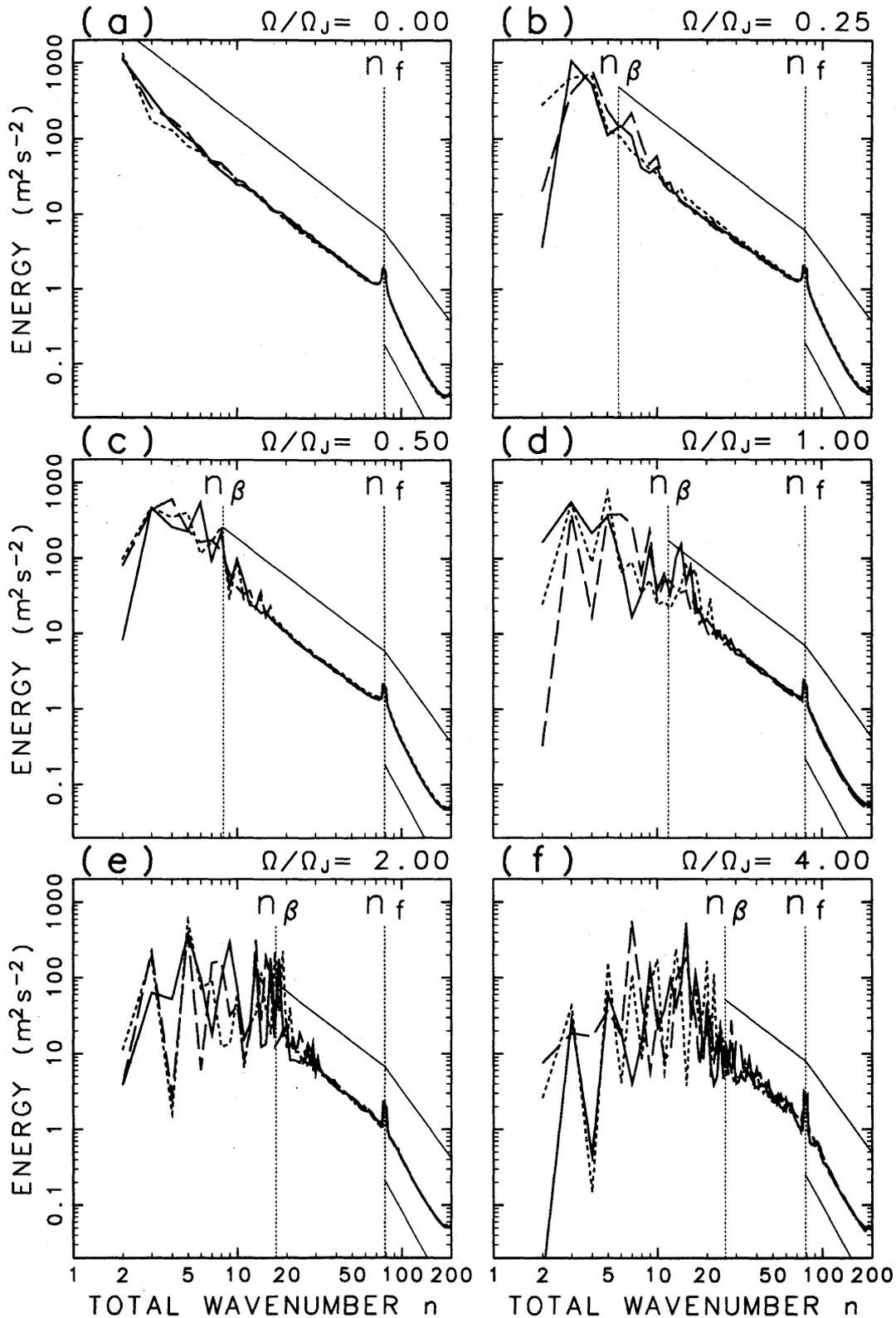
Fig.3: Energy spectrum $\overline{E}(n)$ averaged from 800 to 1000 J.days for six values of $\Omega/\Omega_J$. The forcing wavenumber is indicated by $n_f$ and the wavenumber $n_\beta$ is also indicated, at which scale the "$\beta$-term" is comparable to the nonlinear Jacobian term. Three spectra are plotted for each figure. The spectrum obtained with the same random numbers is plotted with the same line type. A line of $\overline{E}(n) \propto n^{-5/3}$ is added in the range of $n_\beta \le n \le n_f$, and lines of $n^{-3}$ (above) and $n^{-4}$ (below) are also added in the range of $n_f \le n \le N$.

range beyond $n_\beta$. The process of the energy interchange is largely influenced by the rotation. For large $\Omega/\Omega_J$ ($\geq$ 2.00), on the other hand, the energy flux function is not parallel to that of no rotation even in the range of $n_\beta \lesssim n \leq n_f$, indicating that the process of the energy interchange is largely influenced by the rotation even in the energy-cascading range. The energy flux is nearly equal to zero in the lower range of $n \lesssim 6$ for the largest rotation rate ($\Omega/\Omega_J$ = 4.00);little energy is transferred to this range because the energy upward cascade is suppressed by the rotation. This is the reason why the energy density in this range is relatively small for these runs as seen in Fig.3 (f).
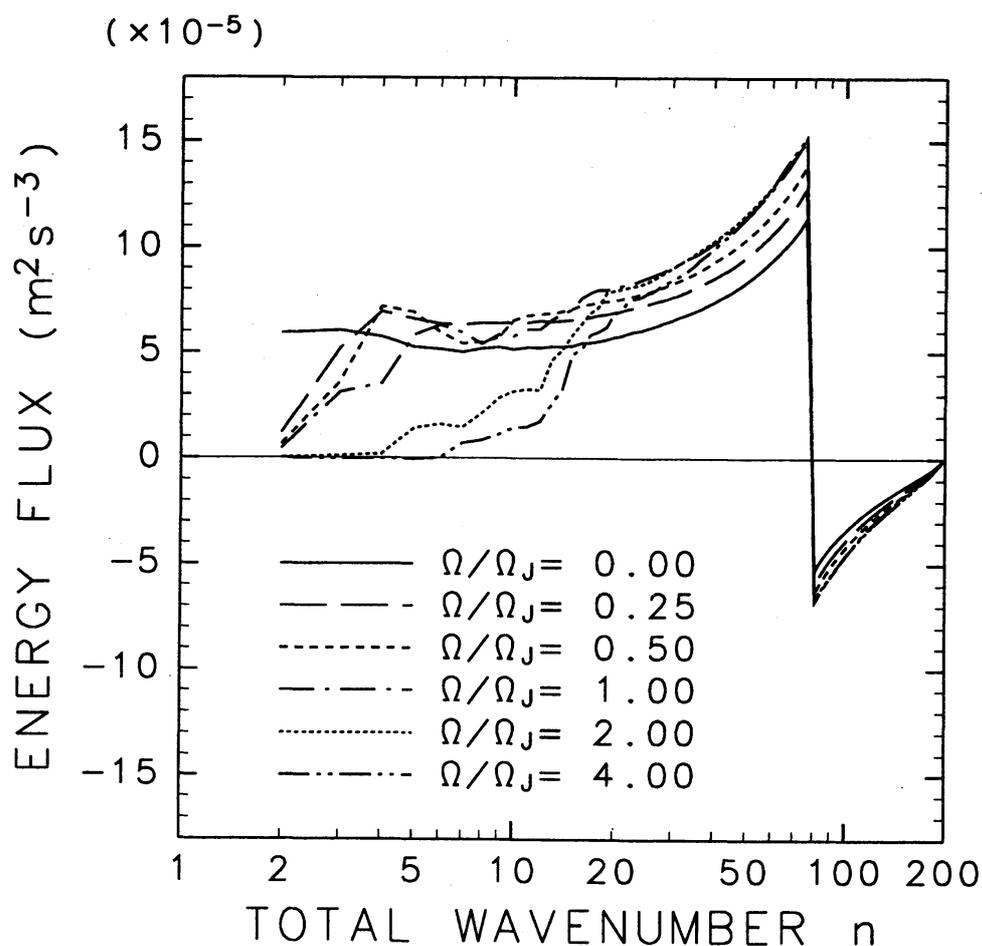


Fig.4: Energy flux function $\overline{\Pi}(n)$ for six values of $\Omega/\Omega_J$. Ensemble averages of three runs.

The streamfunction field at $t$ = 1000 J.days is shown in Fig.5 for six runs. The same random sequance of the vorticity forcing is used for these runs. For the case of no rotation (a), the streamfunction field has a very large pattern which is characterized by the lowest wavenumber $n$ = 2 in consistent with the fact that the transferred energy is accumulating at the lowest wavenumber ( Fig.3 (a), Fig.4 ). This flow pattern moves irregularly on the sphere without changing the pattern largely. For the experiments with rotation (b-f), on the other hand, zonal band structures become dominant in the streamfunction field. As the rotation rate increases, the zonality of the streamfunction field increases. Although details of the flow patterns change with time, the zonal structures are unchanged particularly for large rotation rates.
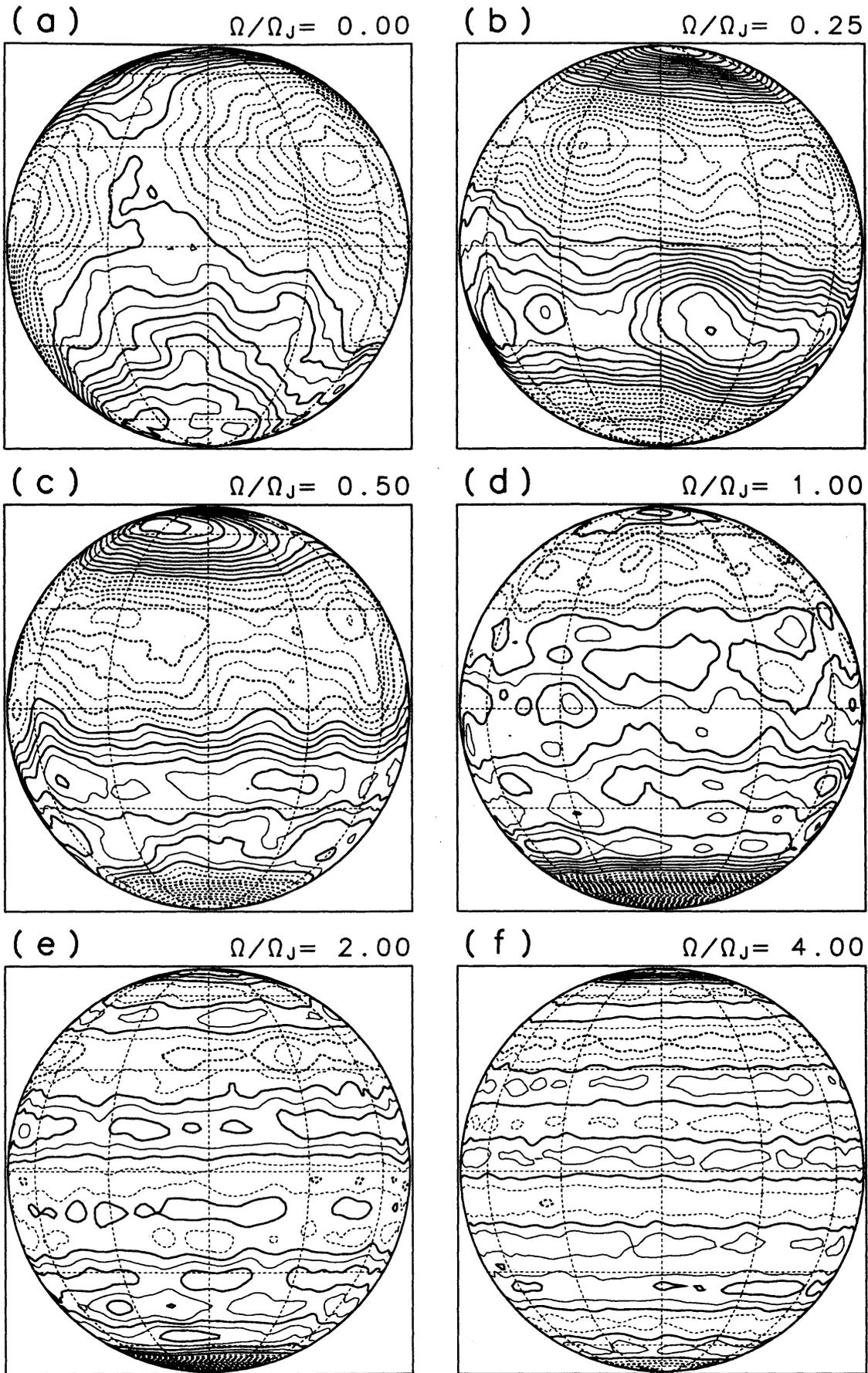
Fig.5: Streamfunction field at $t$ = 1000 J.days for six values of $\Omega/\Omega_J$. Contour interval is $2.5 \times 10^8$ m$^2$s$^{-1}$ and negative areas are drawn by dotted lines.

( a ) $\Omega/\Omega_J=0.00$  0 $3\times10^9(m^2s^{-1})$

90N
60N

30N

EQ

30S

60S
90S

0    200   400   600   800   1000

TIME (J.day)

( b ) $\Omega/\Omega_J=0.25$  0 $3\times10^9(m^2s^{-1})$

90N
60N

30N

EQ

30S

60S
90S

0    200   400   600   800   1000

TIME (J.day)

( c ) $\Omega/\Omega_J=0.50$  0 $3\times10^9(m^2s^{-1})$

90N
60N

30N

EQ

30S

60S
90S

0    200   400   600   800   1000

TIME (J.day)

( d ) $\Omega/\Omega_J=1.00$  0 $3\times10^9(m^2s^{-1})$

90N
60N

30N

EQ

30S

60S
90S

0    200   400   600   800   1000

TIME (J.day)

( e ) $\Omega/\Omega_J=2.00$  0 $3\times10^9(m^2s^{-1})$

90N
60N

30N

EQ

30S

60S
90S

0    200   400   600   800   1000

TIME (J.day)

( f ) $\Omega/\Omega_J=4.00$  0 $3\times10^9(m^2s^{-1})$

90N
60N

30N

EQ

30S

60S
90S

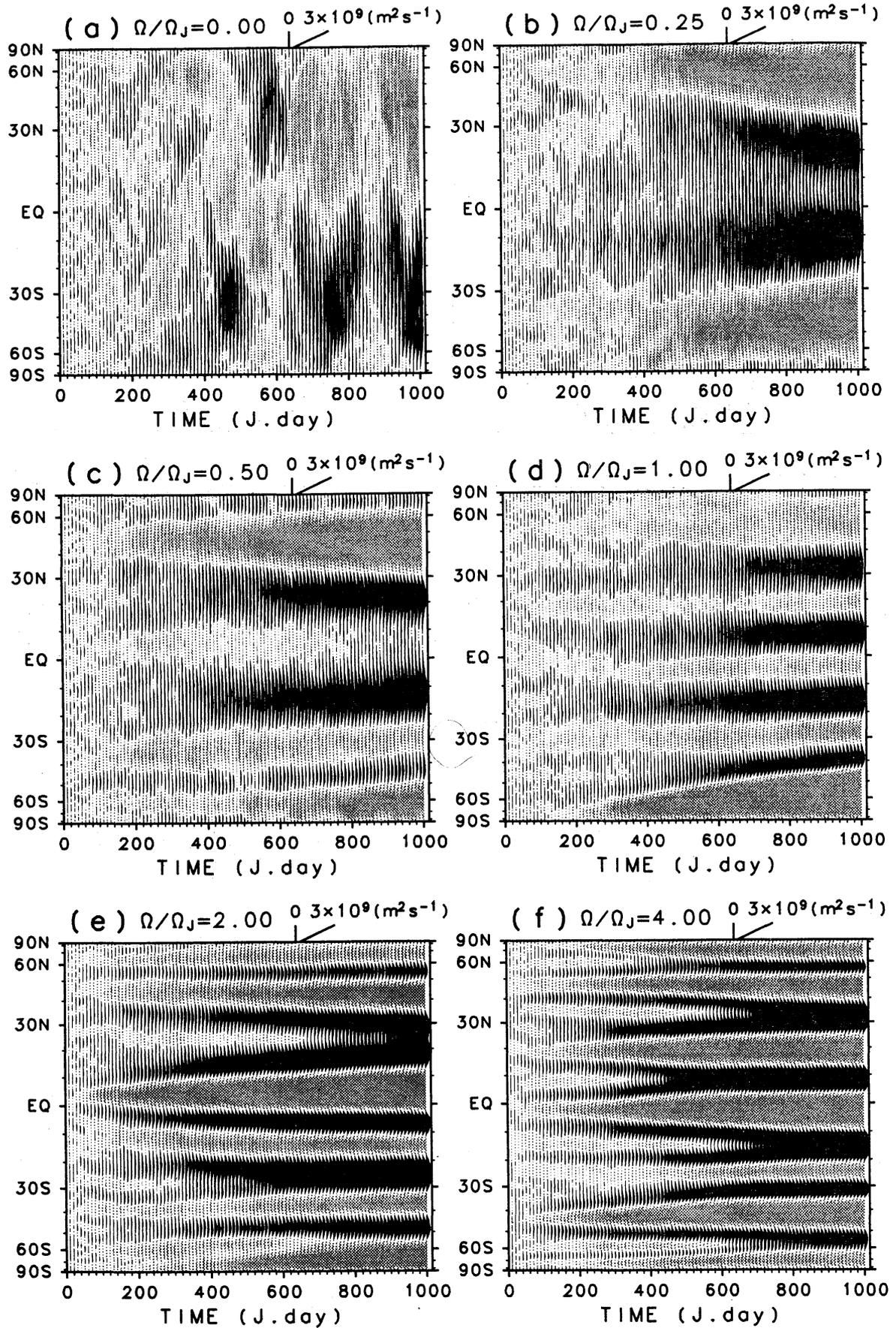0    200   400   600   800   1000

TIME (J.day)

Fig.6: Temporal variation of the zonal mean angular momentum for the same runs as in Fig.5. Time interval is 10 J.days, and the unit of an interval is $3 \times 10^9$ m$^2$s$^{-1}$. Westerly zones are in black while easterly zones in gray.

Figure 6 shows the temporal variation of the zonal mean angular momentum for the same six runs as in Fig.5. For the case of no rotation (a), the intensity of the angular momentum is not very large and the easterly or westerly flow dominates over a hemisphere. Temporal variation of the mean zonal flow is large in consistent with the irregular movement of the flow pattern. For the cases with rotation (b-f), on the other hand, the alternating easterly and westerly bands do not change their positions after the establishment of the band structure. They become clear and robust as the rotation rate increases. They are already discernible in early stages by $t = 100$ J.days. For large $\Omega/\Omega_J$ (e,f), several mergers of westerly bands take place and the width of the bands increases. The number of the bands increases while their width decreases as the rotation rate increases.

Figure 7 (a) shows the time variation of an index of anisotropy $Ai$ introduced by Herring (1975):

$$Ai = \frac{\langle u^2 \rangle - \langle v^2 \rangle}{\langle u^2 \rangle + \langle v^2 \rangle} , \tag{10}$$

where $u(\lambda, \mu, t)$ and $v(\lambda, \mu, t)$ are eastward and northward velocities, respectively, and $\langle \cdots \rangle$ denotes the spherical average. These are ensemble averages of the three runs. For the case of no rotation, the flow field is nearly isotropic ($Ai \sim 0$) throughout the integration time. For the rotating cases, on the other hand, the anisotropy becomes large with time;the flow field increases its zonality ($\langle u^2 \rangle > \langle v^2 \rangle$). The anisotropy increases as the rotation rate increases in consistent with the fact that the streamfunction field has stronger zonality for larger $\Omega$ ( Figs.5 and 6 ). The dependence of $Ai$ on $\Omega/\Omega_J$ at $t = 1000$ J.days is shown in Fig.7 (b). For small rotation rate ($\Omega/\Omega_J < 1.00$), the index of anisotropy is largely different between the three runs but it has a tendency to increase with $\Omega$. For large $\Omega$, on the other hand, $Ai$ is nearly the same for the three runs ($0.8 \sim 0.9$).

Figure 7 (c) shows the time variation of the energy-weighted total wavenumber for the zonal component $n_0$ :

$$n_0 = \sum_{n=2}^{N} n E_0(n,t) / \sum_{n=2}^{N} E_0(n,t) , \tag{11}$$

where $E_0(n, t)$ is the energy density of the zonal component. The wavenumber $n_0$ is a gross measure of the number of the alternating easterly and westerly bands. These are ensemble averages of three runs. For all the runs, $n_0$ decreases sharply by $t \sim 100$ J.days, and it gradually decreases after that. For the last 200 J.days, $n_0$ is nearly constant except for the case of $\Omega = 0.00$. The wavenumber $n_0$ becomes large as $\Omega/\Omega_J$ increases in consistent with the fact that the number of the alternating bands increases with $\Omega/\Omega_J$ as seen in Fig.6. The dependence of $n_0$ on $\Omega/\Omega_J$ at $t = 1000$ J.days is shown in Fig.7 (d), where $n_0$ for the three runs are plotted for each $\Omega/\Omega_J$. The wavenumber $n_0$ is nearly proportional to $\Omega/\Omega_J$ and has little dependence on the choice of the random numbers.

The relative vorticity field at $t = 1000$ J.days is shown in Fig.8 for the same six runs as in Figs.5 and 6. The center of each figure is the same as that in Fig.5. Typical size of the vortices are nearly equal to that of the forcing as seen in Fig.1. For the case of no rotation (a), the vorticity field is isotropic. It also seems to be nearly isotropic for the small and moderate rotation rate (b-d). For large $\Omega$ (e,f), on the other hand, the vorticity field is elongated zonally and the alternating positive and negative vorticity bands emerge. The intensity of the vorticity increases as $\Omega/\Omega_J$ increases in consistent with tha fact that the enstrophy is larger for larger $\Omega/\Omega_J$ as seen in Fig.2 (b).
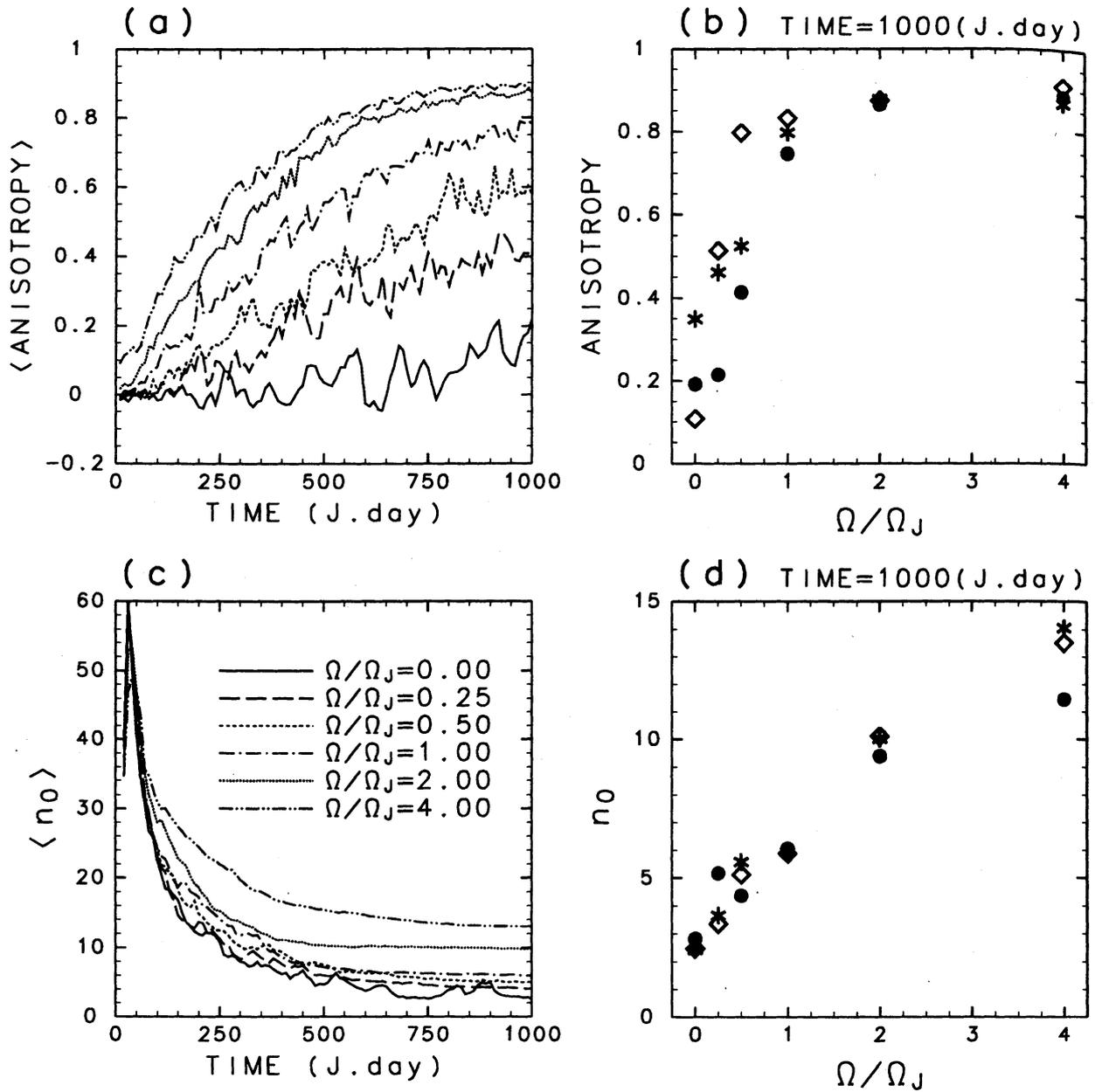
Fig.7: Temporal variation of an index of anisotropy $Ai$ (a), $\Omega/\Omega_J$-dependence of $Ai$ (b), temporal variation of energy-weighted total wavenumber for zonal component $n_0$ (c), and $\Omega/\Omega_J$-dependence of $n_0$ (d). Ensemble averages of three runs in (a,c). Anisotropy $Ai$ and wavenumber $n_0$ obtained with the same random numbers is plotted with the same symbol in (b,d).
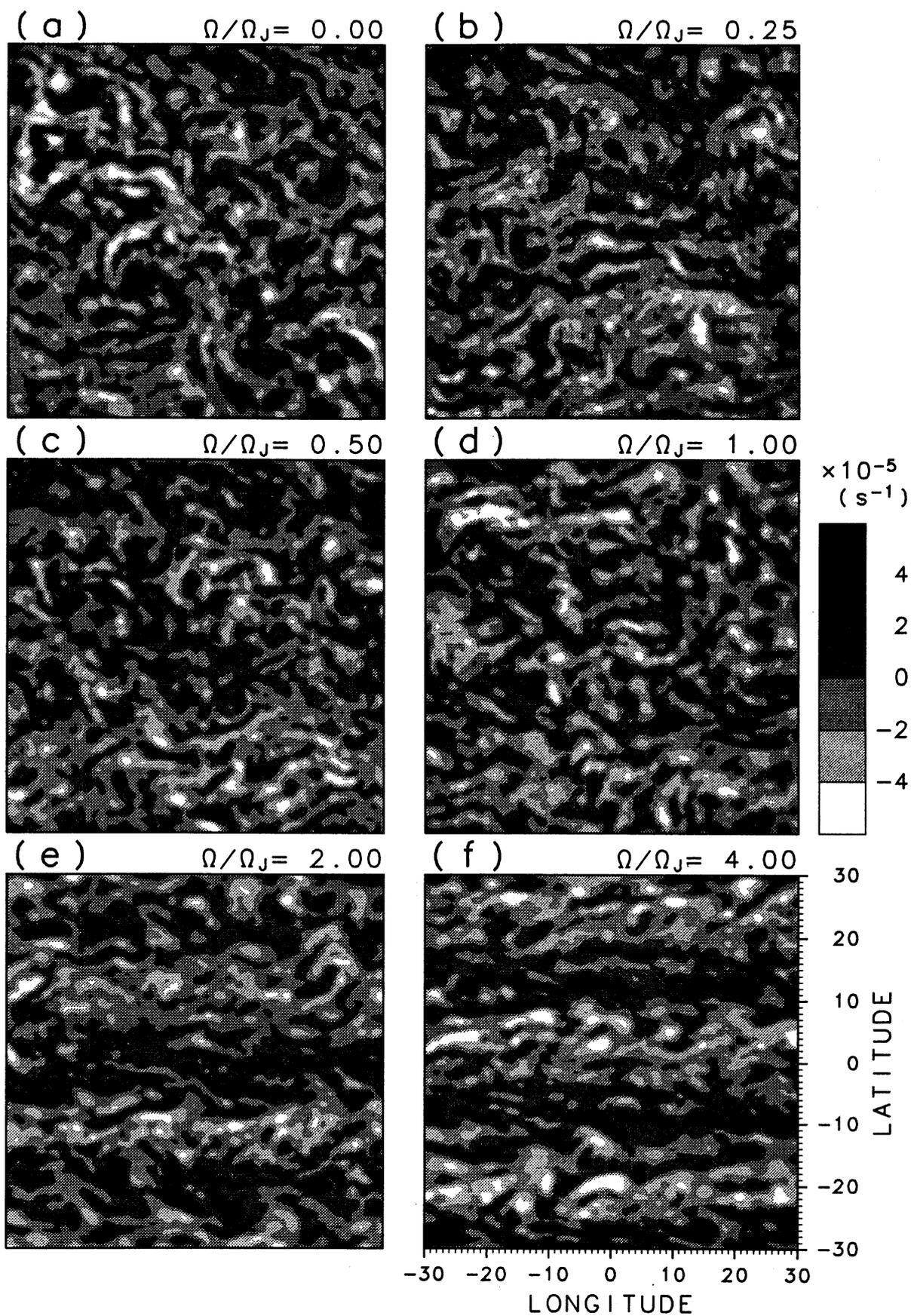
Fig.8: Relative vorticity field at $t = 1000$ J.days for the same runs as in Figs.5 and 6. The center of each figure is the same as in Fig.5.

# 4  Discussion

For the case of no rotation, the energy supplied around $n_f$ is transferred upward and the rate of the energy cascade is nearly constant in the range of $2 \leq n < 20$ as shown in Fig.4, which fact is consistent with the 2D turbulence theory. For the cases with rotation Maltrud and Vallis (1991) has already studied in their numerical experiment on a $\beta$-plane. They showed that the transferred energy accumulates near $k_\beta$ because the upward energy cascade is suppressed by the rotation, and that the power law in the energy-cascading range remains nearly proportional to $k^{-5/3}$. Although the wavenumber $n_\beta$ we used is not identical to $k_\beta$, these features of the energy spectrum influenced by the rotation was obtained in our experiments for small and moderate $\Omega$ ( Fig.3 (b-d), Fig.4 ). For the cases with larger rotation rate $(\Omega/\Omega_J \geq 2.00)$ , on the other hand, the process of the energy interchange is largely influenced by the rotation and the energy is accumulating even in the energy-cascading range. Thus the energy spectrum in this range becomes steeper than $n^{-5/3}$ as shown in Fig.3 (e,f).

Williams (1978) and Nozawa and Yoden (1994) studied the forced two-dimensional turbulence on a rotating sphere with a cyclic boundary condition. Although they showed some impressive clear band structures, the flow field in this study using the isotropic vorticity forcing function does not show such a clear band structures as in our previous study with the same experimental parameters. Thus their results may be influenced by the anisotropic forcing functions and by the cyclic boundary condition.

Yoden and Yamada (1993) studied the decaying 2D turbulence on a rotating sphere, and showed the emergence of strong easterly circumpolar-jets. In this study on the forced 2D turbulence, clear band structures which consist of the alternating easterly and westerly jets appear in all the latitudes, and almost all the circumpolar-jets are easterly ( Fig.6 ). The emergence of easterly jets in high latitudes seems to be a general feature of 2D turbulence on a rotating sphere. Interactions between the mean zonal flow and Rossby waves, of which energy is converted from the turbulent motions by means of the upward energy cascade, seem to be a fundamental dynamics of the formation of the band structure, namely, these Rossby waves might redistribute the zonal mean angular momentum to maintain the band structure.

Nozawa and Yoden (1994) have already studied the organization of the band structure for different random numbers and showed that intensity and width of the jets are not very different, although position of the jets depends on the choice of the random numbers. This is consistent with the fact that the energy-weighted total wavenumber for the zonal component $n_0$ does not largely depend on the choice of the random numbers as shown in Fig.7 (d). The band structure is formed in early stages and then the structure becomes robust and persistent for the cases with rotation as shown in Fig.6 (b-f) (see also Appendix).

# 5  Conclusions

A series of numerical experiments on the forced 2D turbulence on a rotating sphere were done with a high-resolution barotropic model. The formulation of the homogeneous and isotropic vorticity forcing was adopted. Sensitivity of the energy spectrum and the flow field to the rotation rate and that to the choice of the random numbers for the forcing are investigated.

The energy supplied at the forcing wavenumber, $n_f$, cascades upward to low wavenumbers and the enstrophy supplied at $n_f$ cascades downward to high wavenumbers for all the experiments in this study. The upward energy cascade ceases around a wavenumber $n_\beta$ at which the "$\beta$-term" due

to planetary rotation is comparable to the nonlinear Jacobian term. The energy-cascading range becomes narrow as the rotation rate increases, because the upward enrgy cascade ceases around $n_\beta$ and the transferred energy accumulates in the range of $2 \leq n \lesssim n_\beta$. The slope in the energy-cascading range becomes a little steep while it in the enstrophy-cascading range becomes a little gentle as the rotation rate increases, although they remain close to $n^{-5/3}$ and $n^{-4}$, respectively. The energy spectrum in these ranges does not depends on the choice of the random numbers.

For the case of no rotation, the streamfunction field shows a very large flow pattern and the flow field such as the relative vorticity field is isotropic. As the rotation rate increases, zonal band structures become dominant in the streamfunction field;the flow field increases its anisotropy and the number of alternating easterly and westerly bands increases. The band structures are already discernible in early stages and they are robust and persistent for the integration period.

## Appendix

In order to investigate the sensitivity of the zonal band structure to the random sequanses of the vorticity forcing, we perform a series of supplementary experiments. For a certain experiment using a random sequence of I, the random sequence is replaced to that of II after the time $t_c$ J.days, and integrated till $t = 1000$ J.days. Figure A shows the dependence of the zonal mean angular momentum at $t = 1000$ J.days for $\Omega/\Omega_J = 4.00$ on the replaced time $t_c$. The mean zonal angular momentum at $t_c = 1000$ J.days is obtained using full random sequence of I, and that at $t_c = 0$ J.days is using full random sequence of II. The mean zonal angular momentum is almost unchanged for $t_c \geq 180$ J.days;the zonal band structure is already formed by that time and it becomes insensitive to the choice of the random numbers after that time. In high latitudes this timing is earlier than in low and middle latitudes;for example, the band structure is unchanged for $t_c \geq 30$ J.days in southern high latitudes. When the replaced time is very early ($t_c \leq 10$ J.days), the band structure is very sensitive to $t_c$.
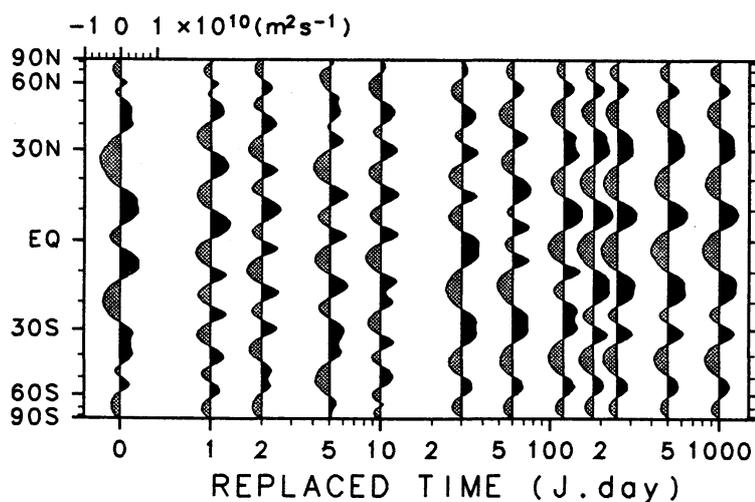


Fig.A: Dependence of zonal mean angular momentum at $t = 1000$ J.days on replaced time $t_c$. $\Omega/\Omega_J = 4.00$.

# References

Basdevant, C., Legras, B., Sadourny, R. & Beland, M. 1981 A study of barotropic model flows : intermittency, waves and predictability. *J. Atmos. Sci.*, **38**, 2305-2326.

Batchelor, G. K. 1969 Computation of the energy spectrum in homogeneous two-dimensional turbulence. *Phys. Fluids*, **12(Suppl. II)**, 233-239.

Boer, G. J. & Shepherd, T. G. 1983 Large-scale two-dimensional turbulence in the atmosphere. *J. Atmos. Sci.*, **40**, 164-184.

Herring, J. R. 1975 Theory of two-dimensional anisotropic turbulence. *J. Atmos. Sci.*, **32**, 2254-2271.

Kraichnan, R. H. 1967 Inertial ranges in two-dimensional turbulence. *Phys. Fluids*, **10**, 1417-1423.

Leith, C. E. 1968 Diffusion approximation for two-dimensional turbulence. *Phys. Fluids*, **11**, 671-673.

Lilly, D. K. 1969 Numerical simulation of two-dimensional turbulence. *Phys. Fluids*, **12(Suppl. II)**, 240-249.

Maltrud, M. E. & Vallis, G. K. 1991 Energy spectra and coherent structures in forced two-dimensional and beta-plane turbulence. *J. Fluid Mech.*, **228**, 321-342.

McWilliams, J. C. 1984 The emergence of isolated coherent vortices in turbulent flow. *J. Fluid Mech.*, **146**, 21-43.

Nozawa, T. & Yoden, S. 1994 A numerical experiment on forced two-dimensional turbulence on a rotating sphere with a longitudinally cyclic boundary condition. **submitted to** *J. Meteor. Soc. Japan.*

Rhines, P. B. 1975 Waves and turbulence on a beta-plane. *J. Fluid Mech.*, **69**, 417-443.

Williams, G. P. 1978 Planetary circulations: 1. Barotropic representation of Jovian and terrestrial turbulence. *J. Atmos. Sci.*, **35**, 1399-1426.

Yoden, S. & Yamada, M. 1993 A numerical experiment on two-dimensional decaying turbulence on a rotating sphere. *J. Atmos. Sci.*, **50**, 631-643.